



Society for Science and Education
United Kingdom

ISSN: 2055 - 1266

Volume 2, No 2, April 2015

JOURNAL OF BIOMEDICAL ENGINEERING AND MEDICAL IMAGING



TABLE OF CONTENTS

EDITORIAL ADVISORY BOARD	I
DISCLAIMER	II
Automatic Vessel Segmentation Based on Region Growing	
Davood Almasi	1
Majid Ghandchi	
Fuzzy-Neuropsychiatric Predictive Model	
Amadin, F. I	14
Obi, J.C.	
Real Time Monitoring of Posture to Improve Ergonomics	
Manju Gopinath	22
Angeline Kirubha	
Comparison of Segmentation Framework on Digital Microscope Images for Acute Lymphoblastic Leukemia Diagnosis using RGB and HSV Color Spaces	
Kamal A. ElDahshan	26
Mohammed I. Youssef	
Emad H. Masameer	
Mohammed A. Mustafa	

EDITORIAL ADVISORY BOARD

Professor Kenji Suzuki

Department of Radiology, University of Chicago
United States

Professor Habib Zaidi

Dept. of Radiology, Div. of Nuclear Medicine, Geneva University Hospital, Geneva, Swaziland

Professor Tzung-Pe

National University of Kaohsiung,, Taiwan
China

Professor Nicoladie Tam

Dept. of Biological Sciences, University of North Texas, Denton, Texas, United States

Professor David J Yang

The University of Texas MD Anderson Cancer Center, Houston
United States

Professor Ge Wang

Biomedical Imaging Center, Rensselaer Polytechnic Institute. Troy, New York
United States

Dr Hafiz M. R. Khan

Department of Biostatistics, Florida International University
United States

Dr Saad Zakko

Director of Nuclear Medicine Dubai Hospital
UAE

Dr Abdul Basit

Malaysia School of Information Technology, Monash University
Malaysia

DISCLAIMER

All the contributions are published in good faith and intentions to promote and encourage research activities around the globe. The contributions are property of their respective authors/owners and the journal is not responsible for any content that hurts someone's views or feelings etc.

Automatic Vessel Segmentation Based on Region Growing

¹Davood Almasi and ²Majid Ghandchi

Department of Technology and Engineering, Islamic Azad University Ahar Branch, Ahar, Iran

¹almasi_d@nicico.com; ²m_ghandchi@iau_ahar.ac.ir

ABSTRACT

Blood vessel segmentation is the fundamental part of many retinopathy diagnoses procedure. In recent years, there has been a substantial amount of work exploring how to utilize the computer analysis of retinal images to automated vessel segmentation. In this paper, we propose a new method based on region growing approach. Firstly, a retinal vessel image is preprocessed by Directional local-contrast filters and LoG-Gabor filter to enhance the vessels' contrast. Then, the region growing method is applied to extract retinal vessels. Comparisons are conducted on the publicly available VIO dataset. Experimental results show that the proposed method reaches the average accuracy of 97.25%, 97.35% and 97.62% on raw image, preprocessed image and mosaic image sets, respectively.

Keywords: Retinal Blood Vessels, Image Segmentation, Region Growing, LoG-Gabor filter.

1 Introduction

Retinal Blood vessels includes the branches and tributaries of the central retinal artery and vein, respectively, and the vascular circle of the optic nerve. Any tiny change in blood vessel structure can be a symptom of a retinal disease. Therefore, blood vessel segmentation is the fundamental part of many retinopathy disease diagnoses. Indirect ophthalmoscopy (IO) is the standard of care for evaluation of the retina. When an ophthalmologist uses an ophthalmoscope to look into the eye he sees the following view of the retina (Figure 1). In the center of the retina is the optic nerve. From the center of the optic nerve radiates the major blood vessels of the retina. Approximately 17 degrees (4.5-5 mm), or two and half disc diameters to the left of the disc, can be seen the slightly oval-shaped, blood vessel-free reddish spot, the fovea, which is at the center of the area known as the macula by ophthalmologists. In Figure 1, retina as seen through an ophthalmoscope and two its main spots are presented.

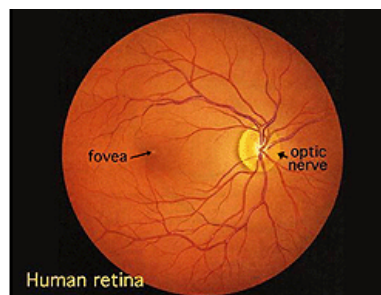


Figure 1: Retina as seen through an ophthalmoscope [1]

Different kinds of methods have been suggested to divide retinal vessels automatically. Prior investigations in [2-4] selected matched filters (MF) to improve retinal vessels, and after that adaptive thresholding are applied to take out vessel pixels. Chaudhuri et al. [3] applied a set of Gaussian kernels to convolve with the retinal images, with this regard that the cross-section of vessels can be nearly modeled as a Gaussian function; afterward they found the maximum response along different directions. Hoover et al. [4], who used region-based threshold probes and local vessel attributes to group pixels as vessels or non-vessels, offered an improvement of MF. Lately, Zhang et al. [2] suggested a MF-FDOG method which was included a zero-mean Gaussian function and the first-order derivative of Gaussian (FDOG). In this procedure, thresholding the image's response to the MF extracted the retinal vessels, yet the image's response to the FDOG must determine the thresholds.

Another group of methods for retinal vessel division is vessel tracking. A method for retinal vessels detection is suggested in [2] which enlarge path-based access into a region-based segmentation plan. They make a forest of tree-like vessel regions by way of a sequence of exploration waves on the vessel map and apply the single-source, multi-destination version of Dijkstra's shortest path algorithm [5].

In [6-8], mathematical morphology approach was used. The authors applied the detected retinal vessel centerlines in [6] to develop vessel structure got from the morphological operations. Combined morphological filters with cross-curvature evaluation was used by Zana et al. [7] to divide vessel-like patterns, and tested this method on retinal photographs. Also, an algorithm based on morphological and topological analysis was suggested by Rossant et al. [8] to extract the vascular tree from eye images.

Supervised learning methods for retinal pixel classification were offered in [9-12]. A simple feature vector for each pixel was extracted by Niemeijer et al. [9], and the K-nearest neighbor (KNN) classifier was used to estimate the probability of each pixel owned by a vessel. A supervised learning method based on the detection of image ridges was offered by Staal et al. [10], which were applied as line elements. In this way, a set of attributes were produced by allotting each pixel to the nearest line element to shape image patches and then a feature selection plan was used to group the pixels. A method based on the pixel's feature vectors was suggested by Soares et al. [11], which were made up of the pixel's intensity and 2D Gabor wavelet transformation responses, and then a Bayesian classifier was applied to get the last retinal vessels. Ricci et al. [12] used two perpendicular line detectors along with the goal pixels to build a attribute vector for vessel pixel categorization by a support vector machine (SVM).

Despite the fact that, these methods have revealed their good functioning for retinal vessel segmentation, there are some limitations must be improved. These limitations are the false extraction for thin vessels, which is because of low contrast between the retinal vessels and the background, and the connectivity loss for the retinal vessel tree, whose topological structure is relatively complex. This paper proposed a new retinal vessel segmentation method based on region growing. Before all else, median and Directional local-contrast filters are applied to remove the non-uniform lighting in VIO images, followed by a LoG-Gabor filter to increase the contrast of the retinal image. After that the retinal vessel segmentation extracted from a fairly poor quality and blur VIO image.

The remaining of this paper is organized as follows. In section 2, we will describe VIO dataset and the properties of VIO images. A major in-depth review of the proposed algorithm including application of

filters and region growing algorithm is presented in section 3. The experimental evaluation and results are presented and discussed in section 4. Finally, conclusions are drawn in section 5.

2 Dataset

In this paper we use the dataset which is collected by Estrada et al. [13] by Video Indirect Ophthalmoscope (VIO) system. VIO system is a relatively economical and convenient imaging system for capturing retinal images during IO evaluations. In VIO, the physician wears a head-mounted video camera during routine IO evaluations. Estrada et al. [13] obtained sixteen VIO videos from six Retinopathy of Prematurity (ROP) examination sessions performed by two ophthalmologists on sixteen different patients at the Neonatal Intensive Care Unit at the Duke University Medical Center in Durham, NC. All the videos were recorded using a Keeler Wireless Digital Indirect Ophthalmoscope.

Unfortunately, several types of artifacts decrease the VIO image quality, including interlacing artifacts, brightness saturation, white or black spots, and distorted colors. A previous study reports that only 24% of these videos can be utilized for Retinopathy of Prematurity (ROP) evaluation with ROPtool [14]. Therefore, innumerable spurious and low quality frames must be removed prior to any form of automated analysis.

Estrada et al. [13] constructed Vessel Extraction in Video Indirect Ophthalmoscopy (VEVIO) dataset which consists of sixteen manually selected frames and sixteen corresponding enhanced large FOV mosaics from sixteen different premature infants. All images are selected from each patient's right eye. After the IO examination, a full mosaic from each video are constructed based on the proposed method in [15].

3 The Proposed Method

As mentioned before, IO images have low quality. Therefore, the preprocessing phase is crucial for vessel segmentation: In the first step of the proposed method the preprocessing functions are applied on input image to remove artificial noises and improve the contrast of vessels. The second step builds the segmented image through region growing vessel segmentation method. Our approach is consisted of two steps which illustrated in Figure 2.

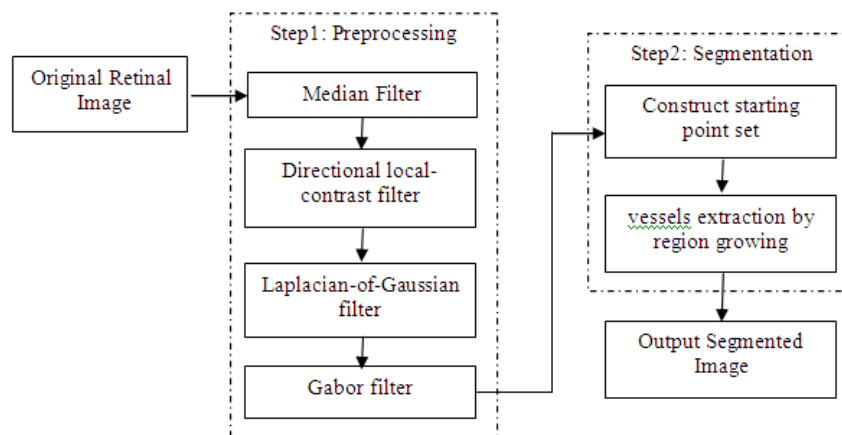


Figure 2: Flowchart of the proposed method

In the following each step will be described in detail.

3.1 Image pre-processing

The main goals of preprocessing step are to remove noise, eliminate artifacts, improve the quality of raw image and increase its contrast. Furthermore, noises and artifacts in mosaic images are accumulated due to frames fusion. In this paper, preprocessing step consists of two stages: Directional local-contrast filters to remove artifacts, LoG-Gabor Filter to improve the contrast of vessels.

3.1.1 Remove artifacts: Median and Directional local-contrast filter

Median and Directional local-contrast filters (DLCF) is used to remove artifacts. Firstly the median filter is applied in image to remove noises. Furthermore, there are some lens artifacts which increase the image's luminance in comparison with the local background. This definition is used to detect and remove the lens artifacts. The Weber measure [16] of contrast is exploited:

$$c_o = \frac{m_o - m_b}{m_b} \quad (1)$$

Where m_o is the median intensity of the object and m_b is the median intensity of the background. The Weber contrast measure is defined for grayscale images. To convert the VIO RGB image to gray scale, the green channel as the standard practice for retinal images [11] is used. m_b is calculated in a small window around each pixel. The size of window must be greater than the size of artifact. The pixel which is identified as an artifact pixel will be substitute by the median value of its surrounding window. As the example picture in Figure 3 shows, this procedure removes white spots from the original image.

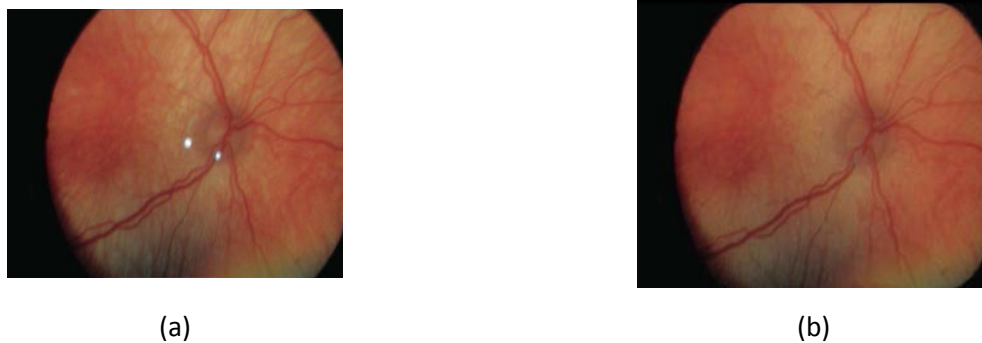


Figure 3: Pixels that are far from the local median brightness are substitute with local median values (a) The original image, (b) The result of directional local contrast filtering.

3.1.2 Improve the contrast of vessels: LoG-Gabor Filter

As mentioned before, VIO images have relatively poor quality, so the vessels are often too unclear and cannot be detected dependably. Thus, the inverted response to a Laplacian-of-Gaussian filter followed by a Gabor filter bank, or LoG-Gabor filter [17] is used to enhance the delectability of vessels in the image. The LoG-Gabor processes the green channel of RGB image due to its ability to represent the best vessel-background contrast.

The LoG filter convolves the image with a LoG operator, which is the result of convolving a low-pass Gaussian filter with a contrast-sensitive Laplace operator:

$$L_{\sigma}(\mathbf{p}; \sigma) = (\nabla^2 \mathbf{N}(\mathbf{p}; \sigma)) * I_g(\mathbf{p}) \quad (2)$$

where $I_g(\mathbf{p})$ is a grayscale version of I , “*” is the convolution operator, and $\mathcal{N}(\mathbf{p};\sigma)$ is an isotropic, zero-mean Gaussian kernel with variance σ^2 . To enhance vessels at different scales, we convolve the original image with filters that vary in the value of their scale parameter σ and retain the maximum response at every pixel:

$$L(\mathbf{p}) = \max_{\sigma} L_{\sigma}(\mathbf{p}; \sigma) \quad (3)$$

Gabor wavelets is used to enhance vessel connectivity. Gabor wavelet filter is defined by multiplying a complex sinusoid by a Gaussian kernel [27]:

$$B(\mathbf{p}; \lambda, \Sigma, \theta) = s(\mathbf{p}; \lambda) \mathcal{N}'(\mathbf{p}; \Sigma, \theta) \quad (4)$$

Where $s(\cdot)$ is the sinusoidal component and $\mathcal{N}'(\cdot)$ is an anisotropic, scaled, and rotated Gaussian function. The LoG filtered image is convolved with filters of varying wavelength (λ), scale (Σ), and orientation (θ), and keep the maximum response at each pixel:

$$G(\mathbf{p}) = \max_{\lambda, \Sigma, \theta} (L(\mathbf{p}) * B(\mathbf{p}; \lambda, \Sigma, \theta)) \quad (5)$$

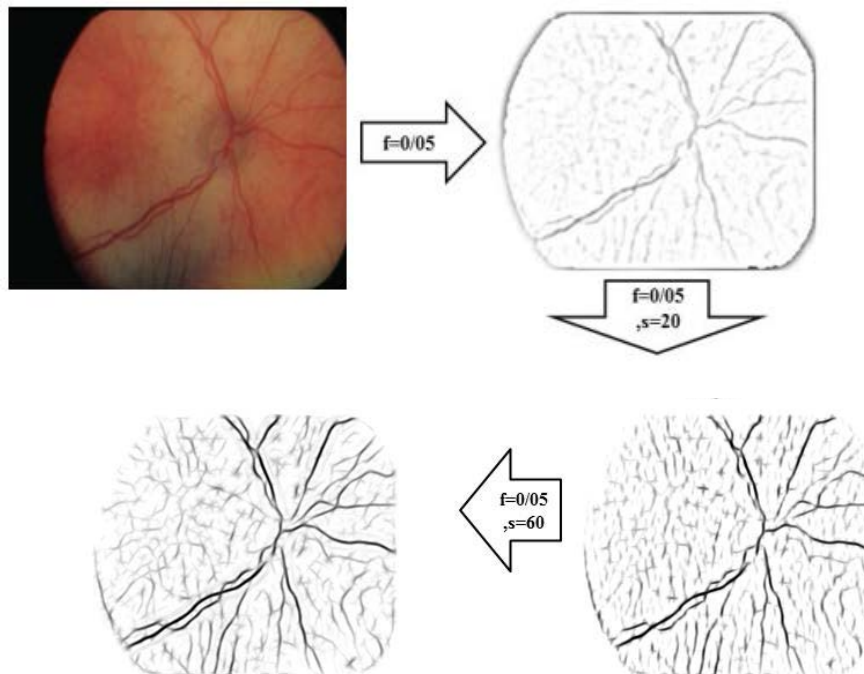


Figure 4: vessel contrast enhancement using LoG-Gabor Filter

3.2 Image Segmentation

After applying the preprocessing steps, image is ready for segmentation. Region growing segmentation method is a method to conquer the failing in segmentation of thin retinal vessels [18]. The region growing to segment these thin curved vessels is applied in this paper [19]. Region growing consist of two level: In first level some starting point is defined and then in the second level the connectivity between each starting pixel and its neighborhoods is calculated.

3.2.1 Feature Extraction and Starting Points

The first stage in segmentation is identifying the pixel features that may distinguish a vessel pixel from a non-vessel pixel. The first feature is the green channel intensity. When the RGB components of the retinal images are pictured one by one, the green channel displays the best vessel-background contrast. The green channel intensity $I_g(\mathbf{p})$ normalized between 0 and 1 and the inverted response $F(\mathbf{p})$ to LoG-Gabor filter arranged in 9 orientations (θ spanning from 0^0 up to 160^0 at steps of 10^0), 2 wavelengths ($= .5, .75$). Thus, the pixel feature vector are composed from two attribute: the green channel intensity $I_g(\mathbf{p})$ normalized between 0 and 1 and the inverted Laplace-Gabor response.

The exploration started from s_0 which:

- is black and the green channel intensity is nearly zero ($I_g(\mathbf{p}) < e$)
- the area intensity is uniform ($I_g(\mathbf{p}) - I_g(\hat{\mathbf{p}}) < e$)
- the inverted response to the LoG-Gabor is nearly zero ($F^{-1}(p) < e$)

We set the parameter e base on our experiment to .0006. In **Error! Reference source not found.** the starting point set included 66 points which are obtained based on these criteria is presented.

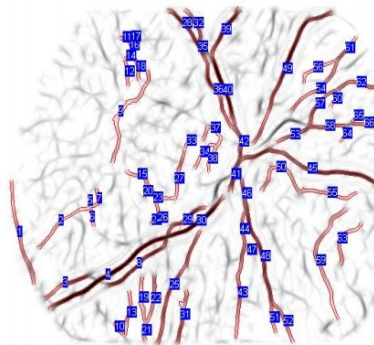


Figure 5: The starting points

3.2.2 Region growing segmentation

The segmentation is initialed from the starting points. All 8-connected neighbors of the starting point will be considered as the vessel, if neighbor $\hat{\mathbf{p}}$, satisfies the similarity criterion, ($I_g(\mathbf{p}) - I_g(\hat{\mathbf{p}}) \ll 1$). $\hat{\mathbf{p}}$ is added to the starting point set, where $I_g(\mathbf{p})$ and $I_g(\hat{\mathbf{p}})$ denote the intensities of the compared neighborhood pixel and the s pixel, respectively.

4 Experimental results

The proposed method is tested on the VIO database [13]. The database has provided manual segmentation for performance evaluation. For the test set, we applied the proposed method on two different sets: A and B. In set A, there are 16 raw VIO images. In first time we apply the region grown algorithm on these raw images and for the second time the complete proposed method are applied on set A. Meanwhile set B consists of the related mosaic images. In this paper, the manual segmented images are used as the ground truth.

For quantitative evaluation of results f-measure, recall, precision and accuracy are used. All of these measures are calculated based on 4 parameters which are widely used in information retrieval:

- true positives (TP) i.e. the number of items correctly labeled as belonging to the positive class.
- true Negative (TN) i.e. the number of items correctly labeled as belonging to the negative class
- false negatives (FN) , which are items which were not labeled as belonging to the positive class but should have been.
- false positives (FP), which are items incorrectly labeled as belonging to the class.

After calculating these four parameters by comparison estimated segmentation images with the manually segmented images which is used as given ground truth segmentation images, the evaluation measurements are calculated.

$$Precision = \frac{TP}{TP + FP} \quad (6)$$

$$recall = \frac{TP}{TP + FN} \quad (7)$$

$$F_Measure = 2 * \frac{Precision * recall}{Precision + recall} \quad (8)$$

$$accuracy = \frac{TP + TN}{TP + FN + FP + TN} \quad (10)$$

4.1 First Experiment

In the first experiment, median and DLC filters are not used and the LOG_Gabor filter is applied on raw VIO images. It is obvious from Figure 6 that noises and artifacts are presented in final segmentation image. Furthermore, it failed to recognize thin vessels. Based on all this facts, this method cannot be a suitable method for vessel segmentation.



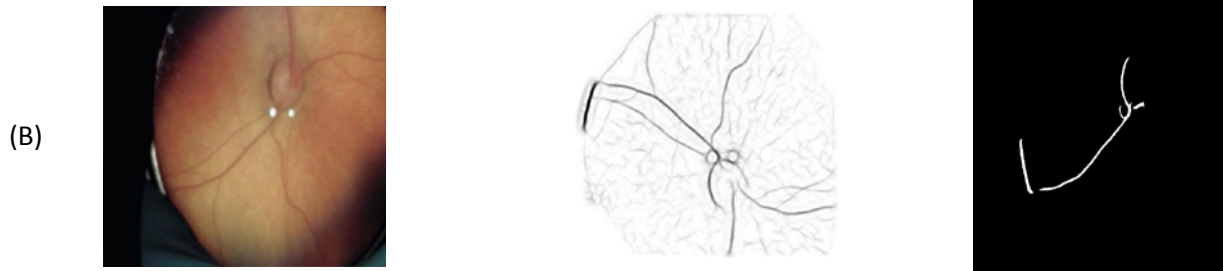


Figure 6: First Experiment. (A). noises and artifacts are presented in final segmentation image. (B) The segmentation method is failed to recognize thin vessels.

The introduced measurements are calculated for first experimental on noisy VIO images. The results are presented in Table 1. The last row of the table indicates the average of each column's values. The average accuracy of the proposed method on this set is about 97.25%.

Table 1: The evaluated measures on noisy VIO images

Image #	FN	FP	TN	TP	Recall	Precision	F_measure	Accuracy
1	3988	0	292908	10304	0.720963	1	0.83786	0.987018
2	12134	0	293452	1614	0.117399	1	0.210129	0.960501
3	7972	0	294600	4628	0.367302	1	0.537265	0.974049
4	9558	0	294023	3619	0.274645	1	0.430936	0.968887
5	5675	0	295432	6093	0.51776	1	0.682269	0.981527
6	4373	0	298476	4351	0.498739	1	0.665545	0.985765
7	6173	0	300013	1014	0.141088	1	0.247287	0.979906
8	16392	0	280873	9935	0.377369	1	0.547957	0.946641
9	2484	0	301495	3221	0.564592	1	0.721712	0.991914
10	6765	0	295222	5213	0.435215	1	0.60648	0.977979
11	15611	0	283943	7646	0.328761	1	0.494839	0.949183
12	10412	0	290027	6761	0.393699	1	0.56497	0.966107
13	7959	0	287467	11774	0.596665	1	0.747389	0.974092
14	11994	0	292340	2866	0.192867	1	0.323367	0.960957
15	6096	0	296481	4623	0.43129	1	0.602659	0.980156
16	7558	0	295050	4592	0.377942	1	0.548561	0.975397
average	8446.5	0	293237.6	5515.875	0.396019	1	0.548076	0.972505

4.2 Second experiment

Median and DLC filters are applied in raw VIO images followed by LOG_Gabor filter for enhancing the VIO images quality and vessel contrast. After applying the proposed segmentation algorithm, the favorable segmentation images are obtained. The results of segmentation algorithm on two images are shown in Figure 7. The images present Figure 7 that artifacts are removed in final segmentation image and thin vessels are extracted successfully.

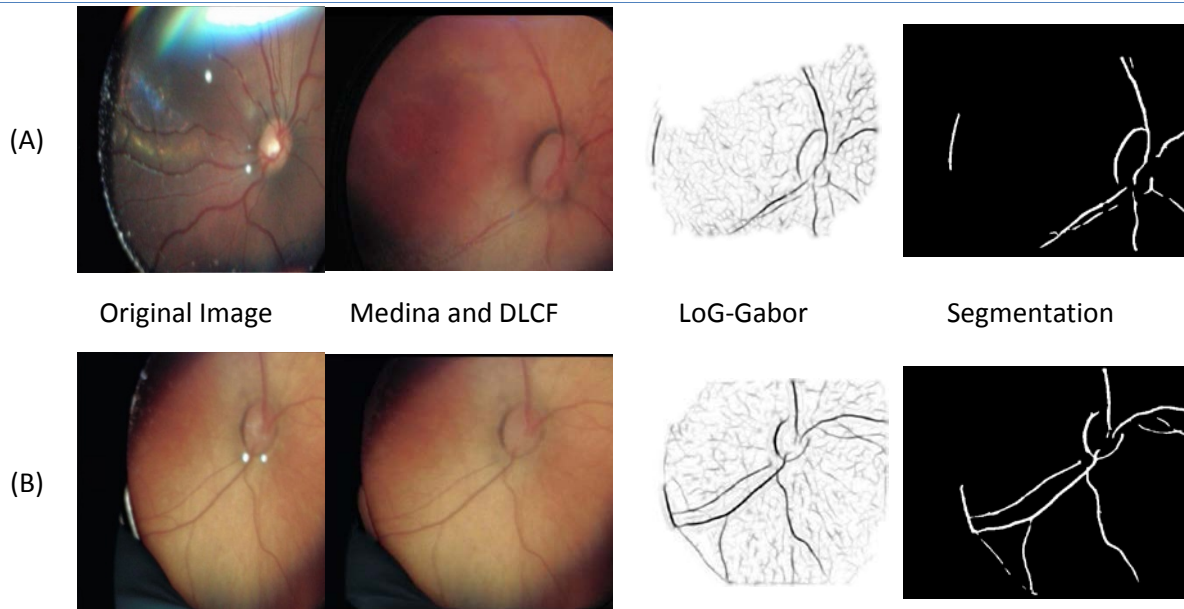


Figure 7: Second Experiment. (A). noises and artifacts are removed in final segmentation image. (B) the segmentation method extract thin vessels

The introduced measurements are calculated for second experimental on preprocessed VIO images. The results are presented in Table 2. The proposed method on this set can obtain the vessels with 97.35% accuracy.

Table 2: The calculated measurements on preprocessed images

Image #	FN	FP	TN	TP	Recall	Precision	F_measure	Accuracy
1	4337	0	292908	9955	0.696544	1	0.821133	0.985882
2	9493	0	293452	4255	0.3095	1	0.472699	0.969098
3	8344	0	294600	4256	0.337778	1	0.504983	0.972839
4	9804	0	294023	3373	0.255976	1	0.407613	0.968086
5	6172	0	295432	5596	0.475527	1	0.644552	0.979909
6	4714	0	298476	4010	0.459652	1	0.62981	0.984655
7	2338	0	300013	4849	0.67469	1	0.805749	0.992389
8	17489	0	280873	8838	0.335701	1	0.502659	0.94307
9	2847	0	301495	2858	0.500964	1	0.667523	0.990732
10	7220	0	295222	4758	0.397228	1	0.568595	0.976497
11	15613	0	283943	7644	0.328675	1	0.494741	0.949176
12	11595	0	290027	5578	0.324812	1	0.490352	0.962256
13	8886	0	287467	10847	0.549688	1	0.709418	0.971074
14	9609	0	292340	5251	0.353365	1	0.522202	0.968721
15	5628	0	296481	5091	0.474951	1	0.644023	0.98168
16	5832	0	295050	6318	0.52	1	0.684211	0.981016
average	8120.063	0	293237.6	5842.313	0.437191	1	0.598141	0.973568

4.3 Third Experiment

The row VIO image has narrow Field of View (FOV), so corresponding enhanced large FOV mosaics are used in this part of our experiment. The quality of these images are improved by applying the mosaicing procedure which is introduced in [15]. the LOG_Gabor filter is applied on mosaic.

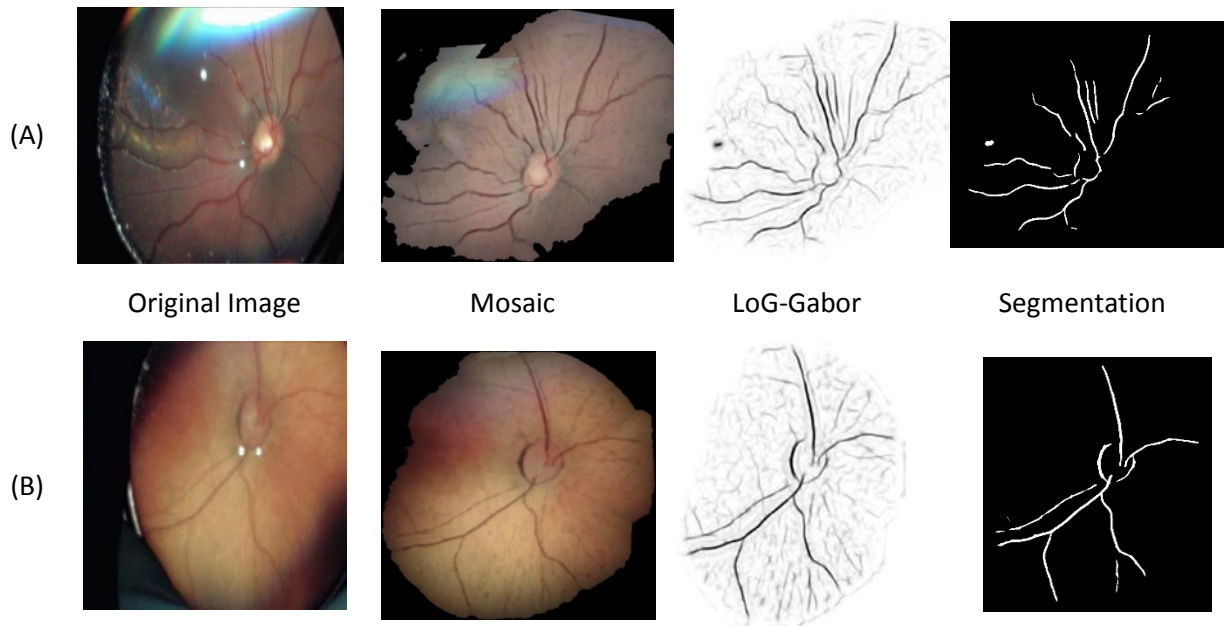


Figure 8: Second experiment on mosaic image

The introduced measurements are calculated for second experimental on mosaics. The results are presented in Table 3. The average accuracy of the proposed method on this set is 97.66% which indicates our method works well on mosaics. On the other hand, mosaics are the best feed for vessel segmentation systems. As indicated in table 3, the tolerance of accuracy is really low.

Table 3: The evaluated measures on mosaics

Image #	FN	FP	TN	TP	Recall	Precision	F_measure	Accuracy
1	8015	0	403929	10606	0.569572	1	0.725767	0.981032
2	5768	0	296517	5515	0.488788	1	0.656626	0.981261
3	7213	0	314258	4959	0.40741	1	0.57895	0.977903
4	7931	0	275146	6485	0.449847	1	0.620544	0.97261
5	7044	0	295298	6824	0.492068	1	0.659579	0.977216
6	7323	0	377165	4912	0.401471	1	0.572928	0.981194
7	6904	0	314946	4660	0.402975	1	0.574458	0.978855
8	12881	0	427213	8479	0.396957	1	0.568317	0.971284
9	7810	0	397748	6642	0.45959	1	0.629753	0.981053
10	8938	0	426166	4576	0.338612	1	0.505915	0.979672
11	17545	0	456524	4923	0.219112	1	0.359461	0.963371
12	6866	0	264176	5438	0.44197	1	0.613009	0.975166
13	11248	0	283331	8622	0.43392	1	0.605223	0.962902
14	8885	0	402182	8079	0.476244	1	0.64521	0.978802
15	7265	0	357443	5977	0.451367	1	0.621989	0.980401
16	7720	0	316168	6824	0.469197	1	0.638712	0.976656
average	8709.75	0	350513.1	350513.1	0.431194	1	0.598527	0.976211

4.4 Comparison of results

A columnar chart is used to comprise the obtained results of three described experiments.

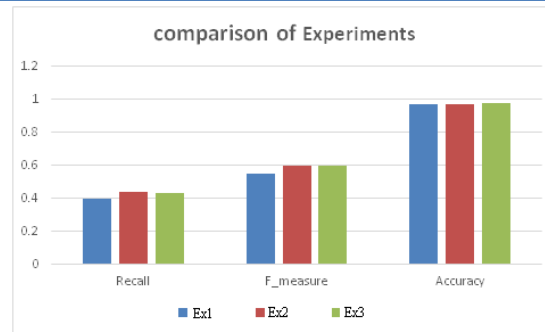


Figure 9: The comparison of experiments

4.5 Comparison the proposed method with other methods

The proposed method is compared with 4 previous works which are mentioned in introduction of this paper. The f-measure and accuracy of the proposed method is higher than the other.

Table 4: comparison the accuracy of the proposed method with other methods

Method's name	F-measure	Accuracy
The proposed method	0.5985	0.9762
Estarda et al.	0.5053	0.9101
Chaudhuri et al.	0.4755	0.9076
Soares et al (GMM).	0.4172	0.9153
Soares et al (KNN).	0.2205	0.9160

5 Discussion

The results we have obtained suggest that the region growing algorithm in conjunction with Gabor filter responses and feature extraction can provide robust blood vessel segmentation while suppressing the backgrounds. Although, the majority of large and small vessels are detected, there are some erroneous false detection of noise and other artifacts when raw VIO image set is used. The major errors are due to background noise and non-uniform illumination across the retinal images. We overcome these difficulties by a set of preprocessing tasks. The precision of the proposed method is quiet well and there is no false positive in segmented images. Therefore all the non-vessel pixels are detected. Furthermore, the accuracy of the proposed method is high, so the segmented vessels are almost the same as actual vessels in the manually segmented images. Finally, the higher accuracy and sensitivity of the proposed method on mosaic images indicate that retinal vessel segmentation will be done better on mosaics.

In conclusion, the advantages of the proposed method can be expressed as follow:

1. The proposed method has high accuracy and high precision in retinal vessel detection.
2. The proposed method initializes with auto finding the starting points.
3. In the proposed method a suitable approach for eliminating distortions and noises is presented.

Indeed, our method, achieves the average accuracy of 97.25%, 97.35% and 97.62% on raw image, preprocessed image and mosaic image sets, respectively.

REFERENCES

- [1] H. Kolb, "Simple anatomy of the retina," *Webvision: The Organization of the Retina and Visual System*, 1995.
- [2] B. Zhang, et al., "Retinal vessel extraction by matched filter with first-order derivative of Gaussian," *Computers in biology and medicine*, vol. 40, pp. 438-445, 2010.
- [3] S. Chaudhuri, et al., "Detection of blood vessels in retinal images using two-dimensional matched filters," *IEEE Transactions on medical imaging*, vol. 8, pp. 263-269, 1989.
- [4] A. Hoover, et al., "Locating blood vessels in retinal images by piecewise threshold probing of a matched filter response," *Medical Imaging, IEEE Transactions on*, vol. 19, pp. 203-210, 2000.
- [5] E. W. Dijkstra, "A note on two problems in connexion with graphs," *Numerische mathematik*, vol. 1, pp. 269-271, 1959.
- [6] A. M. Mendonca and A. Campilho, "Segmentation of retinal blood vessels by combining the detection of centerlines and morphological reconstruction," *Medical Imaging, IEEE Transactions on*, vol. 25, pp. 1200-1213, 2006.
- [7] F. Zana and J.-C. Klein, "Segmentation of vessel-like patterns using mathematical morphology and curvature evaluation," *Image Processing, IEEE Transactions on*, vol. 10, pp. 1010-1019, 2001.
- [8] F. Rossant, et al., "A morphological approach for vessel segmentation in eye fundus images, with quantitative evaluation," *Journal of Medical Imaging and Health Informatics*, vol. 1, pp. 42-49, 2011.
- [9] M. Niemeijer, et al., "Comparative study of retinal vessel segmentation methods on a new publicly available database," in *Medical Imaging 2004*, 2004, pp. 648-656.
- [10] J. Staal, et al., "Ridge-based vessel segmentation in color images of the retina," *Medical Imaging, IEEE Transactions on*, vol. 23, pp. 501-509, 2004.
- [11] J. V. Soares, et al., "Retinal vessel segmentation using the 2-D Gabor wavelet and supervised classification," *Medical Imaging, IEEE Transactions on*, vol. 25, pp. 1214-1222, 2006.
- [12] E. Ricci and R. Perfetti, "Retinal blood vessel segmentation using line operators and support vector classification," *Medical Imaging, IEEE Transactions on*, vol. 26, pp. 1357-1365, 2007.
- [13] R. Estrada, et al., "Exploratory Dijkstra forest based automatic vessel segmentation: applications in video indirect ophthalmoscopy (VIO)," *Biomedical optics express*, vol. 3, pp. 327-339, 2012.

- [14] S. Ahmad, et al., "Computer-assisted assessment of plus disease in retinopathy of prematurity using video indirect ophthalmoscopy images," *Retina*, vol. 28, pp. 1458-1462, 2008.
- [15] R. Estrada, et al., "Enhanced video indirect ophthalmoscopy (VIO) via robust mosaicing," *Biomedical optics express*, vol. 2, pp. 2871-2887, 2011.
- [16] E. Peli, "Contrast in complex images," *JOSA A*, vol. 7, pp. 2032-2040, 1990.
- [17] J. Movellan, "Tutorial on Gabor filters," Open Source Document, <http://mplab.ucsd.edu/wordpress/tutorials/gabor.pdf>, 2002.
- [18] M. E. Martínez-Pérez, et al., "Retinal blood vessel segmentation by means of scale-space analysis and region growing," in *Medical Image Computing and Computer-Assisted Intervention—MICCAI'99*, 1999, pp. 90-97.
- [19] B. N. Subudhi, et al., "Edge Preserving Region Growing for Aerial Color Image Segmentation," in *Intelligent Computing, Communication and Devices*, ed: Springer, 2015, pp. 481-488.

Fuzzy-Neuropsychiatric Predictive Model

Amadin, F. I¹ and Obi, J.C.²

Department of Computer Science, University of Benin, Benin City. Nigeria
frankamadin@uniben.edu¹ and tripplejo2k2@yahoo.com²

ABSTRACT

Due to subjective diagnosis approach, psychiatric diagnosis, prognosis and predication has been tremendously difficult. In short, it has been subjective; tied to a particular human expert with overview on psychiatric diagnosis. Overtimes, inadequate, ineffective and exhaustive medical professional has contributed seriously to poor psychiatric diagnosis. Artificial Intelligence (AI) has shown rich potential in this area. Therefore this research paper has predictively proposed a fuzzy–neural model capable of imprecision or vague handling in collaboration with system self-learning or training using fuzzy logic and neural, subdomain of Soft-Computing (SC) and Artificial intelligence. The various views of the model were visualized using Unified Modeling Language (UML) while system implementation was opened to future research.

Keyword: Fuzzy Logic, Neural Network, Psychiatric, UML

1 Introduction

Mental and behavioral disorders, which results to mental illness have been a major focus by the World Health Organization (WHO, 2004,). Hundreds of millions of people worldwide are affected by mental disorders (Mathers and Lancer 2006). WHO estimates that 154 million people suffer from depression and 25 million people from schizophrenia; 91 million people are affected by Alcohol use disorders and 15 million by drug use disorders (WHO, 2004). As many as 50 million people suffer from epilepsy and 24 million from Alzheimer and other dementias (WHO, 2004). Around 877000 people die by suicide every year³. Within countries, the overall one-year prevalence ranges from 4% to 26% (FMOH, 2004 and WHO, 2004). In high-income countries, depression a lone is likely to be the second highest cause of mental disorders contributing to the overall disease burden.

In Africa and Nigeria as a whole the rate of mental disorder is seriously alarming, this has resulted to serious issues such as stigmatization, disdainful approach and outright insults (FMOH, 2004).

The issues relating to mental health symptoms and correct diagnoses are contained in the International Classification of Mental and Behavioral Disorders (ICD-10) as well as in the Diagnostic Criteria for Research (DCR-10). The successful treatment and interventions require appropriate diagnosis. A major issue faced by psychiatrist is proper diagnosis since symptoms of many mental and behavioral disorders are similar (WHO, 2004).

The fuzzy nature pertaining to the symptoms of varied mental disorder has indeed hinder objective diagnosis and prognosis, leaving room for inadequate or failed diagnosis. Proposing a Neuro-fuzzy,

DOI: 10.14738/jbemi.22.1036

Publication Date: 29th April 2015

URL: <http://dx.doi.org/10.14738/jbemi.22.1036>

Neuro-psychiatric system capable of providing an objective diagnosis cannot be over emphasized which is the centered thrust of this research paper.

2 Review of Related Literature

Neural network (NN) consists of an interconnected group of neurons (Ponniyin, 2009). Artificial Neural Network (ANN) is made up of interconnecting artificial neurons (Programming constructs that mimic the properties of biological neurons). A Neural Network is an analog and parallel computing system. A neural network is made up of a number of very simple processing elements that communicate through a rich set of interconnections with variable weights or strength. ANN (subsequently referred to as NN) is used in solving artificial intelligence problems without creating a model of a real biological system. NN processes information using connectionist approach to computation. It changes its structures based on internal or external information that flows through the network during the learning phase. NN can be used to model complex relationship between input and output or find patterns in data (Gary and George, 2002).

Figure 1 presents a simple NN which comprises of three layers (Input, Hidden and Output layers).

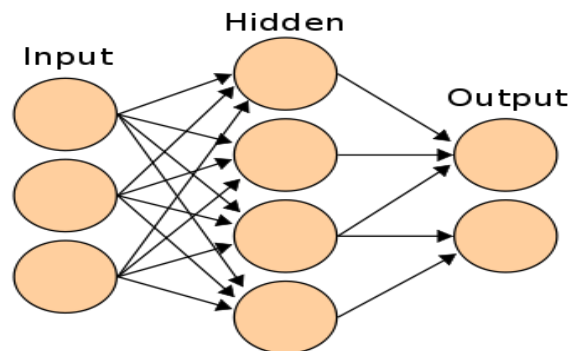


Figure 1: A simple Neural Network (Gary and George, 2002).

The NN presented in Figure 1, comprises of a layer of “input” connected to a layer of “hidden” units, which is in turn connected to a layer of “output” units. The activity of the input unit represents the raw information that is fed into the network; the activity of the hidden units is determined by the activity of the input unit and the weights between the hidden and output units. The hidden units are free to construct their own representation of the input; the weights between the input and hidden units determine when each hidden unit is active, and so by modifying these weights, a hidden unit can choose what it represents (Christos and Dimitros, 2008).

NN employs learning paradigm that includes supervised, unsupervised and reinforcement learning (Christos and Dimitros, 2008). NN has been applied in stock market prediction, credit assignment, monitoring the condition of machinery and medical diagnosis (Dase and Pawar, 2010; Hiroshi et al. 2011; Adyles and Fabricio, 2010; Vahid and Gholam, 2009). Application of NN in medical diagnosis includes electronic noses and diagnosis of cardiovascular systems (Jionghua et al, 2010). NN are ideal in recognizing diseases using scans. They learn by example, hence details of how to recognize the disease is not needed. What is needed is set of examples that are representatives of all the variation of the disease. However, NN cannot handle linguistic information and also cannot manage imprecise or vague information (Jionghua et al, 2010).

Fuzzy Logic (FL) helps computers paint vivid pictures of the uncertain world. Fuzzy sets were introduced by Zadeh (1965) as a means of representing and manipulating data that are not precise, but rather fuzzy. Fuzzy logic provides an inference morphology that helps appropriate human reasoning capabilities to be applied to knowledge-based systems. The theory of fuzzy logic provides a mathematical strength to capture the uncertainties associated with human cognitive processes, such as thinking and reasoning. A fuzzy set A is called trapezoidal fuzzy number (Figure 2) with tolerance interval $[a, b]$, left width α and right width β if its membership function has the following form

$$A(t) = \begin{cases} 1 - (a - t)/\alpha & \text{if } a - \alpha \leq t \leq a \\ 1 & \text{if } a \leq t \leq b \\ 1 - (t - b)/\beta & \text{if } a \leq t \leq b + \beta \\ 0 & \text{otherwise} \end{cases}$$

and we use the notation $A = (a, b, \alpha, \beta)$. It can easily be shown that $[A]^\gamma = [a - (1 - \gamma)\alpha, b + (1 - \gamma)\beta]$, $\forall \gamma \in [0, 1]$. The support of A is $(a - \alpha, b + \beta)$.

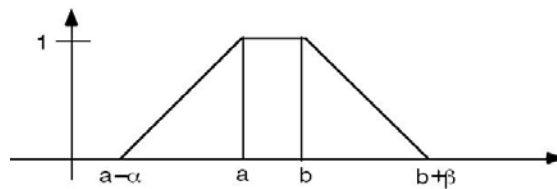


Figure 2: Trapezoidal fuzzy number (Leondes, 2010)

Expert systems are knowledge-based systems that contain expert knowledge. An expert system is a program that can provide expertise for solving problems in a defined application area in the way the experts do. They use human knowledge to solve problems that normally would require human intelligence. These expert systems represent the expertise knowledge as data or rules within the computer. These rules and data can be called upon when needed to solve problems (PCAI, 2002; NIJ 2011 and Steffen 2011).

Fuzzy systems often learn their rules from experts. When no expert gives the rules, adaptive fuzzy systems learn by observing how people regulate real systems (Leondes, 2010). The difference between classical and fuzzy logic is something called “the law of excluded middle” (Bart and Satoru, 1993 and Ahmad, 2011). In standard set theory, an object does or does not belong to a set. There is no middle ground. In such bivalent systems, an object cannot belong to both its set and its complement set or to neither of them. This principle preserves the structure of the logic and avoids the contradiction of object that both is and is not a thing at the same time (Zadeh 1965). However, fuzzy logic is highly abstract and employs heuristic (experiment) requiring human experts to discover rules about data relationship (Angel and Rocio, 2011).

Fuzzy Neural Network or Neuro-Fuzzy system is a learning machine that finds the parameters of a fuzzy system (i.e., fuzzy sets, fuzzy rules) by exploiting approximation techniques from neural networks (Statsoft Incorporated, 2008). Neuro-fuzzy refers to the combination of artificial neural network and fuzzy logic. It eliminates the individual weaknesses of neural network and fuzzy logic while making use of their best advantages. Fusion of neural network and fuzzy logic (that is Neuro-fuzzy) is interesting

(Jionghua et al, 2010; Saman, 2010; Stathacopoulou et al., 2004). Neuro-fuzzy system for the diagnosis of hypotension will provide a self-learning and adaptive system that is able to handle uncertain and imprecise data.

3 Methodology and Design of the Proposed Fuzzy-Neuropsychiatric Predictive Model

The methodology was centered on proposing a Fuzzy-Neuropsychiatric predictive model, which is an architectural framework which enhances the fuzzy (inexact) psychiatric symptoms with the aim of establishing a conclusive boundary point. Unlike the current approaches, in which success or failure are based on the wills and experiences of relevant psychiatric expert personnel designing and administrating the approach in other to elicit relevant diagnosis points. This model is artificial intelligence based; therefore success and failure are not dependent on human intuitions, but success, is closely linked within tuned-up variables within the system components. The model is made-up of five main components as Figure 3 clearly depicts:

- The Input Component (Mental Health Symptoms): The mental health symptoms pertaining to an individual patient is inputted into the system.
- The Processing Fuzzy Membership Component: This component transposes crisp inputted values into fuzzy values for processing optimization.
- Varied Diagnosis Classes: This is usually inferred from the predefined fuzzy rules, breakdown membership function and the exhibited patient symptoms, which will invariably generate a diagnosis class
- Supervised Neural Network: Self-learning and training ability.
- Output: The generated result is transmitted back to the end-user.

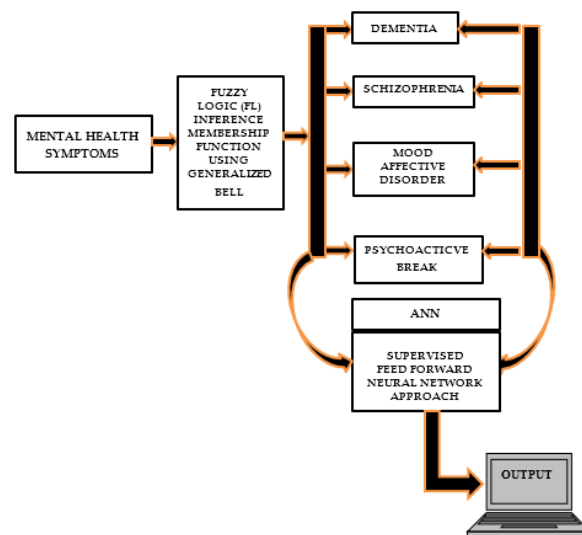


Figure 3: Fuzzy-Neuropsychiatric Predictive Model

3.1 Design

Unified modeling language (UML) is a standard modeling language used for modeling software systems. It provides a number of graphical tools that can be used to visualize a system from different viewpoints.

The multiple views (user, structural, behavior, implementation and environment) of the system that is represented by using diagrams together depict the model of the system (Philippe, 2000 and Chris, 2000). The views typically used are The User view; represents the goal and objectives of the system form user’s viewpoint. The structured view; represent the static or idle state of the system. The behavioral view; represents the dynamic or changing aspect of the system. The implementation view; represents the distribution of the logical elements, such as source code structure, runtime implementation structure of the system. The environment view; represents the distribution of the physical elements of the system.

The Unified Modeling Language is used to illustrate the processes involved in the design and implementation of the model. The model is represented using the following UML diagram specified from Figure 4 -8.

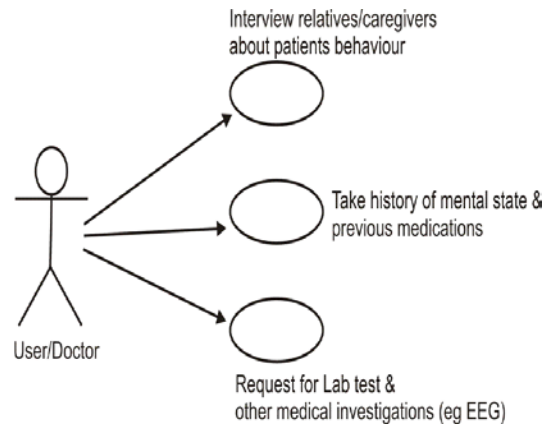


Figure 4: Use-Case Diagram for the Fuzzy-Neuropsychiatric predictive model

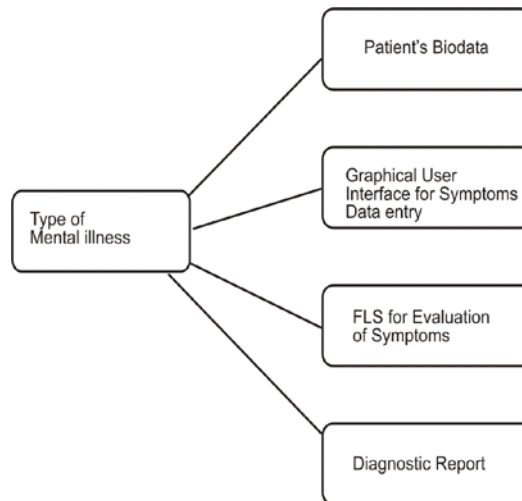


Figure 5: Class Diagram for the Fuzzy-Neuropsychiatric predictive model

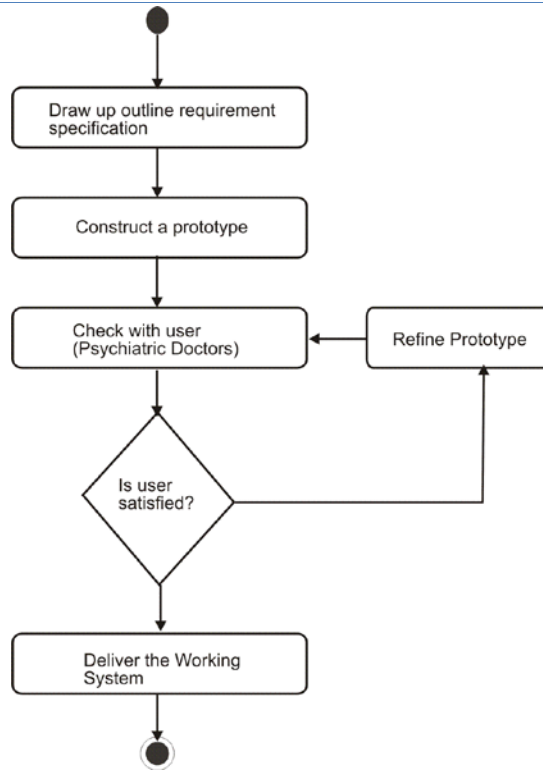


Figure 6: Activity Diagram for the Fuzzy-Neuropsychiatric predictive model

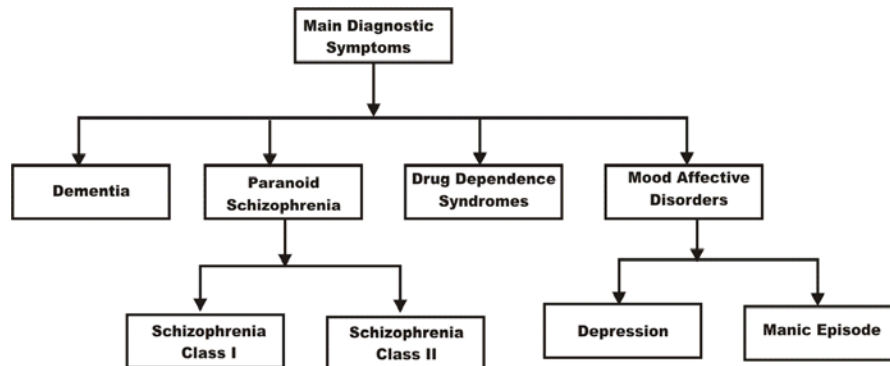


Figure 7: Hierarchy Input-Processing-Output Chart (HIPO) for the Fuzzy-Neuropsychiatric predictive model

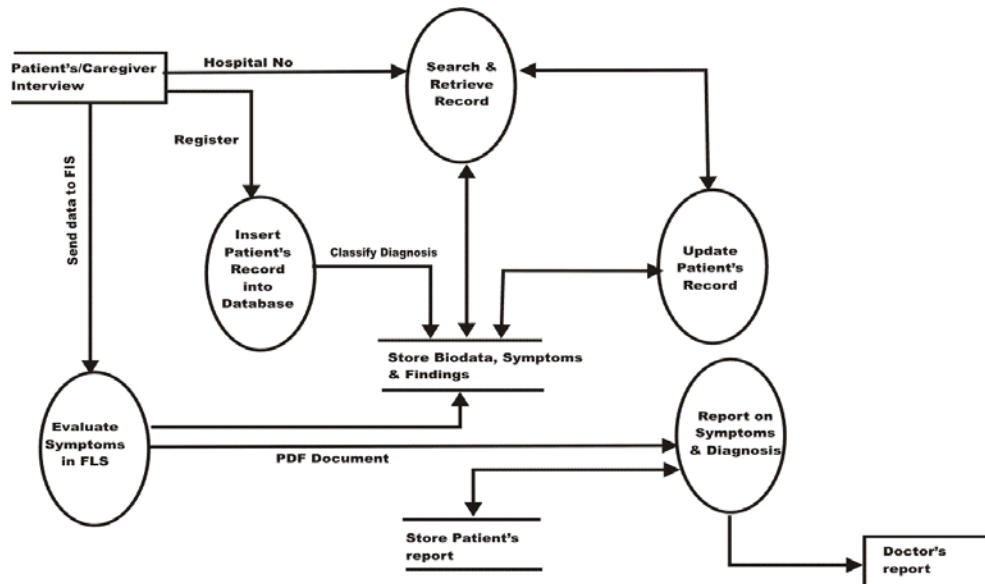


Figure 8: Data Flow Diagram (DFD for the Fuzzy-Neuropsychiatric predictive model)

4 Discussion

The utilization of UML as a design tool has indeed visualized various aspect of the system from the user view down to the interface and even system implementation phase. This design approach will foster easily system implementation

5 Conclusions

A Fuzzy-Neuropsychiatric Predictive Model has been proposed and designed utilizing an informal design tool (UML), highlighting the fuzzy system components and interaction. On full system implementation of the various Artificial Intelligence (AI) techniques, objective diagnosis will have suppressed subject approach, providing a conclusive fuzzy boundary for early, gradual and optimal result.

REFERENCE

- [1] Adyles A. J., Fabricio C. L. A. (2010), "Automatic Faults Diagnosis by Application of Neural Network System and Condition-based Monitoring Using Vibration Signals, retrieved from <http://www.informatics.org.cn/doc/ucit201001/ucit20100104.pdf>
- [2] Angel C. and Rocio R. (2011), "Documentation management with Ant colony Optimization Metaheuristic: A Fuzzy Text Clustering Approach Using Pheromone trails" retrieved from soft computing in Industrial applications, Advances in intelligent and soft Computing, 2011 vol. 96, 2011, 261-70, DOI: 10.1007/978-3-642-20505-1_23
- [3] Christos S. and Dimitros S. (2008), "Neural Network" retrieved from <http://docs.toc.com/doc/1505/neural-networks>.
- [4] Dase R.K. and Pawar D.D. (2010), "Application of Neural network to stock market prediction: A review of literature", retrieved from <http://www.bioinfo.in/uploadfiles/12843>

- [5] FMOH (2004), Revised National Health Policy, Federal Ministry of Health, Abuja
- [6] Gary R. and George P.E. (2002), "Application of Neuro System to behavior Representation in Computer generated forces", retrieved <http://www.Cuil.com>
- [7] Hiroshi S.; Kentaro K.; Kazuo O. and Masato O. (2011), "Statistical mechanics of Structural and temporal credit assignment effects on learning in neural Networks" retrieved from <http://pre.aps.org/abstract/PRE/v83/i5/e051125> .
- [8] Jionghua T.; Suhuan W.; Jingzhou Z. and Xue W. (2010), "Neuro-fuzzy logic based fusion algorithm of medical images" retrieved from http://ieeexplore.ieee.org/xpl/freeabs_all.jsp
- [9] Leondes C. (2010), "The Technology of Fuzzy Logic Algorithm retrieved from Suite101.com/examples-of-expert-System-application-in-artificialIntelligence.
- [10] Mathers C.O. and Lancer D. (2006), Projections of global mortality and burden of disease from 2002 to 2030, *Plus Medicine*, 3: 2011-2030
- [11] NIJ: National Institute of Justice (2011), "Expert system technologies for criminal justice application" retrieved from <https://www.ncjrs.gov/pdffiles1/nij/sl000959.pdf>
- [12] PCAI (2000), "Expert System: Introduction, retrieved from http://www.pcai.com/web/ai_info/expert.systems.html.
- [13] Ponniiyin S.K. (2009), "Neural Network", lcan2007.org/neural.networks.
- [14] Saman K. H. (2010), "Neuro-Fuzzy Systems from the Neural Network Perspective" retrieved from <http://citeseerx.ist.psu.edu/viewdoc/summary?doi=10.1.1.39.857>
- [15] Statsoft Incorporated (2008), "Neural Network" retrieved from <http://google.com>.
- [16] Steffen L. (2011), "Expert system and local Computation", University of Oxford, Graduate Lectures Hilary Term 2011
- [17] Stathacopoulou R.,Magoulas G.D.,Grigoriadou M., and Samarakou M. (2004), "A Neuro-Fuzzy Approach to Detect Student's Motivation, retrieved from http://et.teiath.gr/English/cv/cv_samarakou.html-
- [18] Vahid K. and Gholam A.M. (2009), "Artificial Intelligence in medicines" V47, Issues 1 Information Technology Department, School of Engineering, Terbiat Moderas University Tehran, Iran.
- [19] WHO (2004), World Health Report; changing history. Geneva, World Health Organization.
- [20] Zadeh L.A. (1965), "Fuzzy sets. Information and control, Vol.8, pp.338-353.

Real Time Monitoring of Posture to Improve Ergonomics

¹Manju Gopinath and ²Angeline Kirubha

Department of Biomedical Engineering, SRM University, India

¹manju_gopinath@srmuniv.edu.in; ²angeline.sp@ktr.srmuniv.ac.in

ABSTRACT

Back pain is one of humanities most frequent complaints. While dangerous diseases are being combatted on a daily basis, something as simple as bad posture is often overlooked. Bad posture can start off as a simple habit and soon lead to chronic back pain. Thus it is essential to maintain an ideal posture so as to reduce stress on the body. In this paper, monitoring of posture is done using flex sensor placed along the spine to detect the movement or bend. As posture changes from 'ideal' to 'poor', the user is alerted through a buzzer and LCD. A microcontroller is used to set the limits of ideal posture, which can be user specific. A load cell is used to monitor the variation in body weight and spine stress for poor and ideal postures under sitting and standing cases. The proposed system aims to implement a simple posture monitoring and correction system that can be set up at the work place with ease. This can serve to prevent cases of scoliosis and other spine issues which often start with poor posture.

Keywords: posture; flex sensor; load cell; ergonomics.

1 Introduction

Back pain is one of humanities most frequent complaints. In industrialized countries 80 % of the population will experience back pain at some point in their life. The number of people with back pain increases with advancing age, starting in school children and peaking in adults of 35 to 55 years of age [1].

Ideal posture indicates proper alignment of the body's segments such that least amount of energy is required to maintain a desired position. Good posture optimizes breathing and improves the circulation of bodily fluids [2].

After a time, poor posture feels normal and continues to regress further from the correct posture. When poor posture feels normal to a person, it becomes harder to correct because the muscle memory now stores the information needed for poor posture and disposes of the memory for correct posture [3]. Poor posture will continue to digress the longer it is left uncorrected. With a simple posture monitoring and correcting system as described in this paper, one can monitor the posture easily and thereby correct it on the long run.

2 The Existing Systems

The existing systems for posture monitoring are complicated systems with markers and IR cameras set up and incorporates a gait lab for posture evaluation. Such a system is difficult to set up for continuous

DOI: 10.14738/jbemi.22.1160

Publication Date: 2nd May 2015

URL: <http://dx.doi.org/10.14738/jbemi.22.1160>

monitoring of posture. Other systems use accelerometers and gyroscopes placed on the patients back and shoulders to detect the spine movement. However, the data obtained tends to be too sensitive to properly monitor the postures [4]. Smart vests have been developed for posture monitoring where inductive sensors were sown into a t-shirt. But drawbacks include motion artifacts and wearability of the t-shirt designed [5].

3 Methodology and Design

3.1 Block Diagram of Proposed System

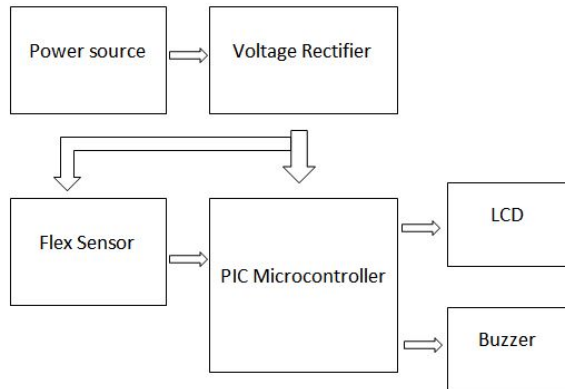


Figure1. Block Diagram of Flex Sensor Module

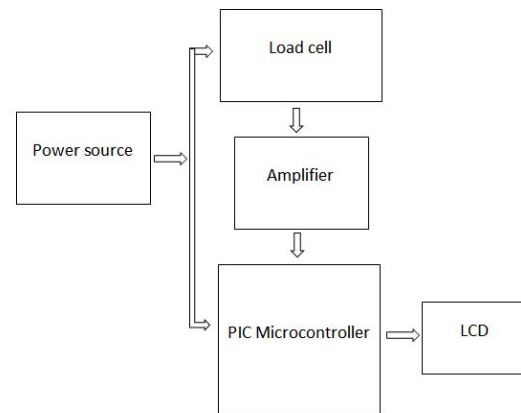


Figure 2. Block Diagram of Load Cell Module

A flex sensor is placed on the subject's back along the curve of the spine in the mid thoracic region. A load cell is placed between platforms on which the subject can stand. Signals from the flex sensor and the load cell are sent to a microcontroller with a built in analog to digital conversion. The microcontroller is programmed to monitor the posture and check for deviation from normal posture and sound the buzzer as an alert. The flex sensor and load cell values are displayed on the LCD. The values are also sent to a computer to store and analyze at a later point of time.

3.2 Detecting Spine Variation using Flex Sensor

As the person bends their spine, the flex sensor also bends, causing a change in resistance which is converted to voltage values and digitalized. The microcontroller has a user defined threshold limit which can be determined by trial and error for each subject individually. The microcontroller detects the posture variation and sounds the buzzer when the subjects posture exceeds the threshold limit set by the user. As different people have different body types and spine curvatures, the threshold limit is set depending on the patients comfort level and can be adjusted as required.

3.3 Detecting the Load Variation using Load Cells

A load sensor is used to measure the stress that is being exerted on the spine while posture varies from ideal to poor. By this, the subject can determine how much change in load is present on the spine and the whole body. Load cell reading is taken for sitting and standing position and the variation in load while posture is altered can be determined. The values are displayed on an LCD and also sent to a computer to store and analyze at a later point of time.

4 Experiment and Analysis

The flex sensors were positioned on the mid thoracic region for optimal detection and threshold was determined under a relaxed posture while sitting. The posture variation was tested by bending the spine to mimic poor posture condition. The load cell was placed under a platform on which the subject would stand. The variation in load was tested for sitting and standing condition under poor and ideal posture.

Table 1. Detection of Poor Posture under various placements of the sensor.

Sensor Placement	Threshold Range [0 to 50]	Detection of Poor Posture
Upper Thoracic	45	Buzzer sounds when >45
Lower Thoracic	42	42 – 45 Unable to detect
Mid Back	47	Detects from 45
Lumbar	Not definable	Not detectable

Sensor placement is best suited for upper thoracic or mid back, depending on the subject. For lower thoracic and lumbar regions, flex sensor is not sensitive enough to detect the bend in spine adequately.

Table 2. Variation of Load under Poor and Normal Posture for Sitting Position.

Subject	Weight (kg)	Load in Good Posture (N)	Load in Poor Posture (N)	% Increase in Load on Spine
S1	52	431.5	433.2	0.39
S2	57	461	464	0.65
S3	63	490	492.6	0.53

Table 3. Variation of Load under Poor and Normal Posture for Standing Position.

Subject	Weight (kg)	Load in Good Posture (N)	Load in Poor Posture (N)	% Increase in Load on Spine
S1	52	510	519.8	1.92
S2	57	560	581	3.75
S3	63	618	637.5	3.15

During detection of load variation, subjects were made to maintain position without any voluntary movements for proper measurement.

5 Conclusion

We were able to implement a simple posture monitoring and correction system using flex sensor and load cell. Flex sensor can be used as a detection of poor posture applicable for cases of scoliosis and other thoracic abnormalities. Load cell readings indicate that 85% of the body weight is on the buttocks while sitting compared to standing.

In sitting position, poor posture affects the load on the spine by 0.52% increase in load. In standing position, poor posture has a much more prominent affect, increasing the load on spine by 2.94%. Using the proposed system, posture can be monitored on a continuous basis and load applied on the spine can be minimized.

In the future work, the system can be improved to wirelessly transmit the data to a computer for analysis. The system can also be made more compact so as to monitor posture for additional activities

such as walking, running, etc. A custom made flex sensor of greater length will be able to detect variation of entire spine curvature instead of being limited to a small region.

REFERENCES

- [1] Institute for Health Metrics and Evaluation. "2010 Global Burden of Disease Study".
- [2] A Patient's Guide to Rehabilitation for Low Back Pain: Understanding the Neutral Spine Position.
- [3] Sullivan, Karin Horgan, Jan 1999, 'Perfect Posture', Vegetarian Times 257, p.64.
- [4] Bilal El-Sayed, et al., (2011) 'A Novel Mobile Wireless Sensing System for Realtime Monitoring of Posture and Spine Stress', 1st Middle East Conference on Biomedical Engineering (MECBME)
- [5] Emilio Sardini, et al., 'Smart Vest for Posture Monitoring in Rehabilitation Exercises', Sensors Applications Symposium (SAS), IEEE.

Comparison of Segmentation Framework on Digital Microscope Images for Acute Lymphoblastic Leukemia Diagnosis using RGB and HSV Color Spaces

¹Kamal A. ElDahshan, ²Mohammed I. Youssef, ³Emad H. Masameer, ⁴Mohammed A. Mustafa

^{1,3}Mathematics Department, Faculty of Science, AL-AZHAR University, Cairo, Egypt;

²Electronic Engineering Department, Faculty of Engineering, AL-AZHAR University, Cairo, Egypt;

⁴MIS Department, Modern Academy for Computer Science and Information Technology, Cairo, Egypt;

dahshan@gmail.com; mohiyosof@yahoo.com; emadmasameer@yahoo.com;
mohammedsecret@gmail.com

ABSTRACT

Image segmentation process is considered the most essential step in image analysis especially in the medical field. In this paper, the color segmentation for acute lymphoblastic leukemia images (ALL) is applied to segment each leukemia image into two clearly defined regions: blasts and background. The ALL segmentation process is based on two different color spaces: RGB color space and HSV color space. The comparison performance between the segmentation methods based on RGB and HSV color spaces are investigated to find the best method to segment the acute lymphoblastic leukemia images. The experimental results show that the segmentation of ALL images based on HSV color space yield better accuracy than RGB color space when compared with the manual segmentation image made by medical experts. Using HSV color space, the shape of blasts in ALL blood samples is closely preserved with segmentation accuracy over 99.00%. However, segmentation based HSV color space was chosen as it produced the highest ALL segmentation rate.

Keywords: Image Segmentation, Microscope Images, ALL, RGB, HSV.

1 Introduction

Leukemia disease is a group of cancers resulting from abnormal increase of the white blood cells that divided and grew in uncontrolled way. Thousands of people all over the world die of leukemia every year that is caused by the nature of Leukemia cells that become out of control and spread independently as well. Early diagnosis and treatment applied to the correct cells are vital.

Leukemia can be classified into two main categories: acute and chronic. Acute leukemia spreads very quickly and has to be treated immediately rather than chronic leukemia where immediate treatment is not a must. Acute leukemia can be either lymphoblastic (ALL) or myelogenous (AML), based on affected cell type. Chronic leukemia can be either lymphoblastic (CLL) or myelogenous (CML) [1]. Acute lymphoblastic leukemia (ALL) is considered to be the prime focus of this work because the survival rate here is expected to be higher when compared to AML.

Segmentation is one of the most demanding tasks in image processing. It is used in Computer Vision to automatically divide a digital image into a number of different meaningful regions. For biomedical imaging applications, image segmentation is a founding step in image analysis as it will directly affect the post-processing. It is a crucial component in diagnosis [2] and treatment [3].

The main aim of acute leukemia blood cell segmentation is to extract component such as blast from its complicated blood cells background. There are many techniques that have been developed for image segmentation such as threshold techniques [4], clustering technique [5] and watershed clustering [6]. Due to the complex nature of blood cells and overlapping between these cells, segmenting them remains a challenging task [7]. Many algorithms for segmentation have been developed for color images that produce more information of the scene than grayscale images do [8].

For leukemia segmentation process, transformations of original RGB images to different color spaces such as (HSI, HSV, YUV, XYZ, Lab...etc.) are proposed in many works. According to [9], Lab color space is used for segmentation process. Also, algorithm Based on HSI color space is proposed in [10]. Based on HSV color space, segmentation technique [11] for ALL images is proposed. This work focuses on RGB and HSV color spaces for acute lymphoblastic leukemia segmentation.

2 Methodology

2.1 Image Dataset

Microscope Images of ALL are taken from ALL-IDB database [12]. An optical laboratory microscope together with a Canon Power Shot G5 camera was used to capture the images of the database. In addition, all images are in JPG format with 24 bit color depth, resolution 2592×1944 . Moreover, the images are taken with different magnifications of the microscope ranging from 300 to 500. ALL-IDB2 version of the database is used as well. Figure 1 shows the sample of ALL images.

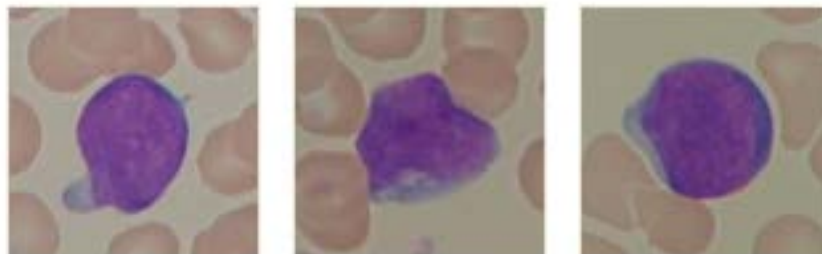


Figure 1: Sample of ALL images

2.2 Segmentation Based RGB Color Space

The main goal is to use RGB color space in segmentation of acute lymphoblastic leukemia images to extract blasts from background. There are 4 steps involved in applying image segmentation process based on RGB color space as shown in figure 2.

- Step1: Apply the contrast enhancement technique namely local contrast stretching (LCS) on the original acute lymphoblastic leukemia image.
- Step2: Select the threshold value by using histogram.

- Step3: Apply the 7×7 median filter.
- Step4: Display the resulted image in RGB color space.

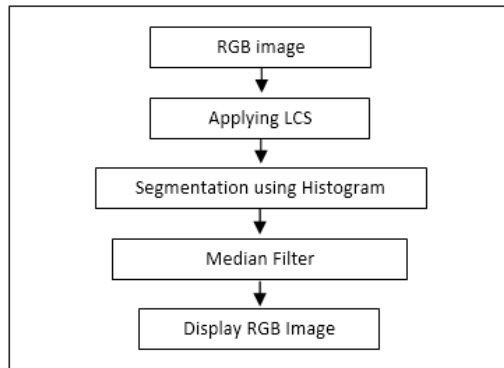


Figure 2: Block diagram of segmentation using RGB

Local contrast stretching is a preprocessing enhancement technique that is applied on an ALL image for adjusting each image element value locally for visualization improvement. LCS is performed by the convolution of the kernel across the image and adjusting the center element using the following formula:

$$I_p(x, y) = 255 \cdot [I_o(x, y) - \min] / (\max - \min) \quad (1)$$

Where:

$I_p(x, y)$ is the color level for the output pixel(x, y) after the LCS process.

$I_o(x, y)$ is the color level input for data the pixel(x, y).

\max - is the maximum value for color level in the input image.

\min - is the minimum value for color level in the input image.

According to formula, (x, y) are the coordinates of the center picture element in the kernel and \min and \max are the minimum and maximum values of the image data in the selected kernel [13].

LCS considers each range of color channel (R, G and B) in the ALL image separately. The range of each color channel will be used for contrast stretching process to represent each range of color. This will give each color channel a set of \min and \max values [14].

2.3 Segmentation Based HSV Color Space

HSV color space is a nonlinear transformation of RGB color space. The representation of HSV cone is shown in figure 3.

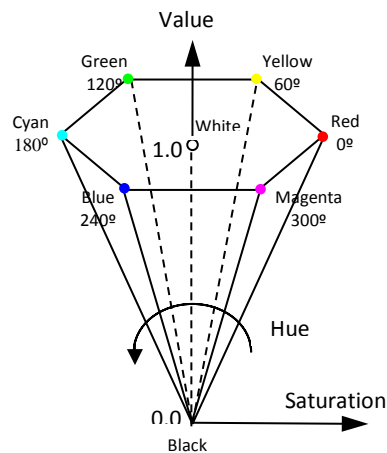


Figure 3: HSV color space

The hue (H) channel refers to the color type such as (Red, Green, Yellow...etc.). The range of hue values changes from 0° to 360° passing through rainbow colors as shown in figure 4.

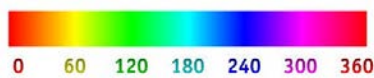


Figure 4: Hue Scale

Saturation (S) value affects the purity of the colors while Value (V) means the amount of light in the color. Both S and V range from 0 to 1. Transformation the source RGB color space to HSV color space is performed based on the following equations:

$$H = \begin{cases} 0 & \text{if } M = m \\ \left(60^\circ \times \frac{g - b}{M - m} + 0^\circ\right) \bmod 360^\circ & \text{if } M = r \\ 60^\circ \times \frac{b - r}{M - m} + 120^\circ & \text{if } M = g \\ 60^\circ \times \frac{r - g}{M - m} + 240^\circ & \text{if } M = b \end{cases}$$

$$S = \begin{cases} 0 & \text{if } M = 0 \\ \frac{M - m}{M} = 1 - \frac{m}{M} & \text{otherwise} \end{cases},$$

$$V = M$$

Where:

M means the maximum values in *R*, *G*, and *B* elements.

m means the minimum values in *R*, *G*, and *B* elements.

The ultimate goal of ALL segmentation is to extract component such as blast from its complicated blood cells background by using HSV color space. There are 6 steps involved in applying image segmentation process as shown in figure 5.

Step 1: transform the source RGB color space to HSV color space.

Step 2: extract H channel from HSV color space.

Step 3: Select color range of nucleus and cytoplasm by using color histogram of H channel. Two angle values A1, A2 are obtained from color histogram for segmentation using multilevel thresholding.

Step 4: Implement the median filter $N \times N$ ($N = 7$) to the resulted images.

Step 5: Synthesize the HSV image.

Step 6: Convert the HSV image to RGB to display.

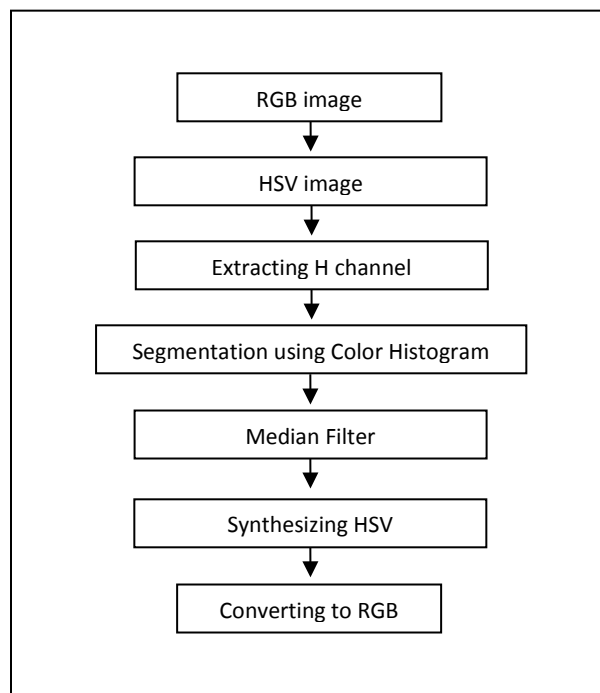


Figure 5: Block diagram of segmentation using HSV

3 Results and Discussion

In this study, image segmentation framework using RGB and HSV color spaces have been applied on two acute lymphoblastic leukemia images labeled as a and b. The quality of segmented images has been determined based on both qualitative and quantitative evaluations.

3.1 Qualitative Analysis

The original acute lymphoblastic leukemia images are shown in figure 6(a), (b). Based on these ALL images, the morphologies of blasts are hardly seen due to the low images contrast.

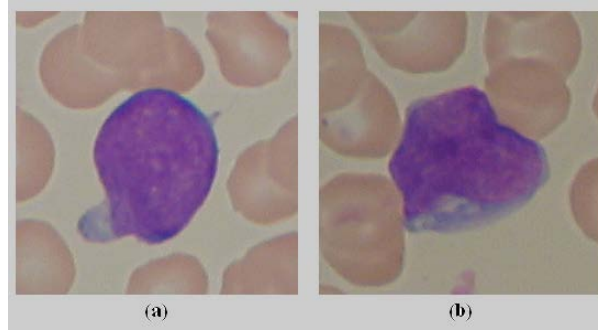


Figure 6: Original RGB images

For segmentation framework based RGB color space, the results of applying the local contrast stretching technique on (a), (b) leukemia images are shown in Figure7 (a), (b) with histogram respectively. Based on these resultant images, the contrast of blast (cytoplasm and nucleus) and background regions has been improved significantly compared to the original images. Also, the LCS histogram of two images is used to select the threshold value.

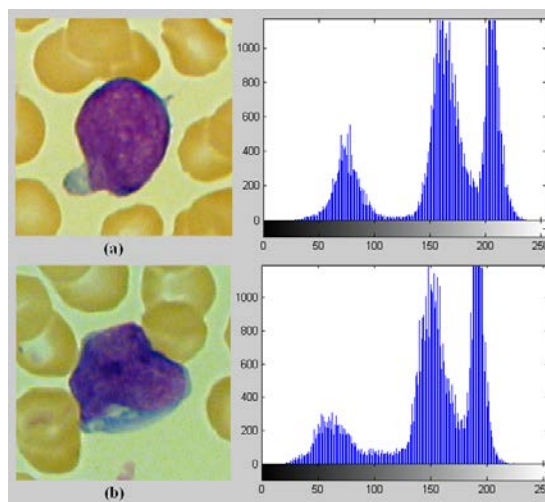


Figure 7: LCS and histogram of RGB images

The results obtained in Figure 8 shows that the elimination of all cytoplasm blast after segmentation using RGB color space. Figure 9 shows the ghost of segmented images using RGB color space that contains cytoplasm blast and background.

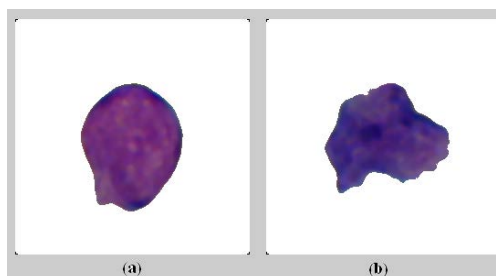


Figure 8: Segmented images using RGB

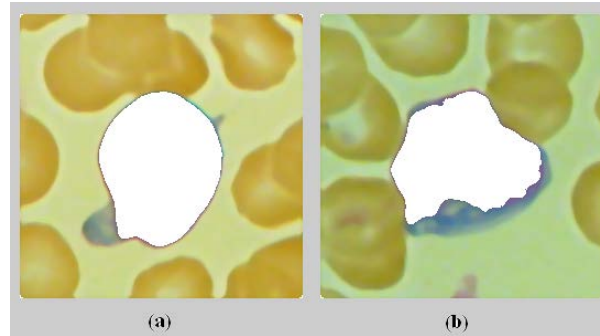


Figure 9: Ghost images for RGB segmentation

According to figure 10, the equivalent HSV images are represented. Meanwhile, Figures 11 shows the color histogram of h channel that used to obtain multilevel thresholding values.

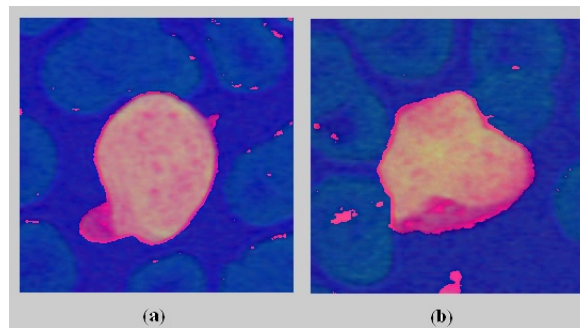


Figure 10: Equivalent HSV images

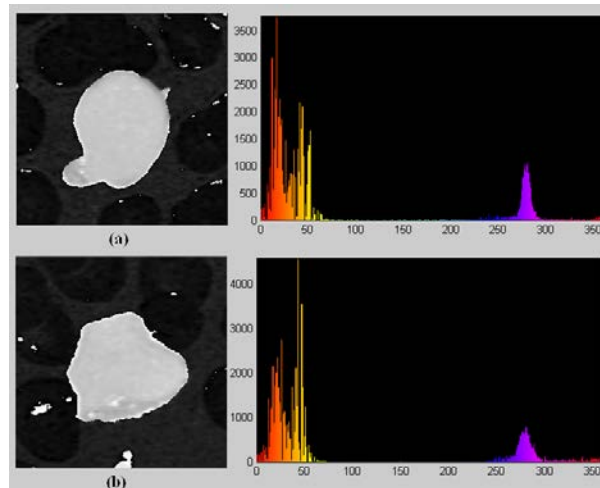


Figure 11: H channel color histogram of HSV images

Figure 12 illustrate the segmented images using an HSV color space which seems to overcome the problem of cytoplasm elimination caused by segmentation based RGB color space. The ghost of segmented images using HSV color space is shown in figure 13.

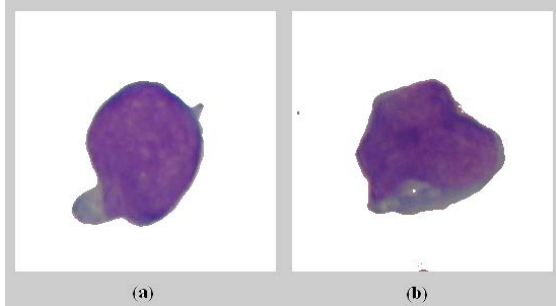


Figure 12: Segmented images using HSV

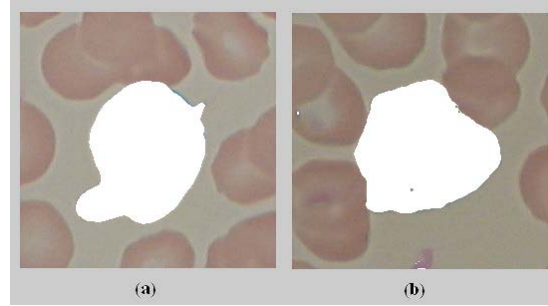


Figure 13: Ghost images for HSV segmentation

Therefore, Figure 12 (a), (b) indicates that the shape of the blasts resulted from segmentation based HSV color space yields almost similar shape to Figure 6 (a), (b) respectively whereas the shape from Figure 8 (a), (b) is quite dissimilar.

3.2 Quantitative Analysis

The quality of segmented ALL images using RGB and HSV color spaces is determined statistically based on global quantitative method. Area pixels of the resultant segmented ALL images is compared to manual segmented image made by medical experts as reference. Table 1 tabulates the segmentation performances based on RGB and HSV color spaces.

Table1: Segmentation performances of ALL images based on RGB and HSV color spaces

Image Label	Segmentation results in pixels			Performances (%)	
	Manual	RGB	HSV	RGB	HSV
(a)	52140	54459	52596	95.74	99.13
(b)	51624	55456	52034	93.09	99.21

4 Conclusion

In this work, a performance comparison between image segmentation framework by using RGB and HSV color spaces for ALL blast detection is performed. The results obtained from segmentation based on hue channel of HSV color space provide almost similar pixel values when compared to manual segmentation with average accuracy about 99.17%. While the segmentation based on RGB gives average accuracy about 94.42% which mean that it has not performed well. The results also show that the color histogram of hue channel is also useful for the selection of the multilevel thresholding values using HSV color space. In the future, the result of this work can be used as the basis for features extraction from the acute lymphoblastic leukemia blood samples.

REFERENCES

- [1] G. C. C. Lim, Overview of Cancer in Malaysia. Japanese Journal of Clinical Oncology, Department of Radiotherapy and Oncology, Hospital Kuala Lumpur, Kuala Lumpur, Malaysia, 2002.
- [2] P. Taylor, Invited review: computer aids for decision-making in diagnostic radiology - a literature review. Brit. J. Radiol.,1995. 68:945–957.

- [3] V.S. Khoo, et al, Magnetic resonance imaging (MRI): considerations and applications in radiotherapy treatment planning. *Radiother. Oncol.*, 1997. 42:1–15.
- [4] Q. Liao, Y. Deng, An Accurate Segmentation Method for White Blood Cell Images. In *IEEE International Symposium on Biomedical Imaging*, 2002. pp.245-248.
- [5] V. Piuri, F. Scotti, Morphology Classification of Blood Leucocytes by Microscope Images. In *IEEE International Conference on Computational Intelligence International Conference on Image, Speech and Signal Analysis*, 2004. pp. 530–533.
- [6] N. Venkateswaran, Y. V. Ramana Rao, K-means Clustering Based Image Compression in Wavelet Domain. *Journal of Information Technology*;, 2007. 148-153.
- [7] S. Mao-jun, et al, A New Method for Blood Cell Image Segmentation and Counting Based on PCNN and Autowave. in *ISCCSP*, 2008. Malta.
- [8] Aimi Salihah , A.N, M.Y.Mashor , Nor Hazlyna Harun, Colour Image Enhancement Techniques for Acute Leukemia Blood Cell Morphological Features. *IEEE*, 2010. pp.3677-3682.
- [9] S. Mohapatra and D. Patra, Automated Cell Nucleus Segmentation and Acute Leukemia Detection in Blood Microscopic Images. in *International Conference On Systems In Medicine and Biology* ,2010. India.
- [10] N. H. A. Halim, et al, Nucleus segmentation technique for acute leukemia. In *Proceedings of the IEEE 7th International Colloquium on Signal Processing and Its Applications*, 2011. (CSPA '11) pp. 192–197.
- [11] K.A. Eldahshan, et al, Segmentation Framework on Digital Microscope Images for Acute Lymphoblastic Leukemia Diagnosis based on HSV Color Space. *International Journal of Computer Applications*, 2014. 90(7): 2014.48-51.
- [12] R. Donida Labati, V. Piuri, F. Scotti, ALL-IDB: the Acute Lymphoblastic Leukemia Image DataBase for image processing., 2011.
- [13] I. Attas, J. Belward, A variational approach to the radiometric enhancement of digital imagery. *IEEE Trans, Image Process*, 1995. 4(6) 845-849.
- [14] N.R.Mokhtar, et al, Contrast Enhancement of Acute Leukemia Images Using Local and Global Contrast Stretching Algorithms. *ICPE*, 2008.